Geochemistry Geophysics Geosystems G3
AN ELECTRONIC JOURNAL OF THE EARTH SCIENCES
Published by AGU and the Geochemical Society

Article
Volume 9, Number 4
2 April 2008
Q04005, doi:10.1029/2007GC001816
ISSN: 1525-2027

Antarctic sediment chronology by programmed-temperature pyrolysis: Methodology and data treatment

Brad E. Rosenheim
National Ocean Sciences Accelerator Mass Spectrometer Facility, Woods Hole Oceanographic Institution, Woods Hole, Massachusetts, USA

Now at Department of Earth and Environmental Sciences, Tulane University, New Orleans, Louisiana 70118, USA (brosenhe@tulane.edu)

Mary Beth Day
Department of Geosciences, Hamilton College, Clinton, New York, USA

Now at Graduate Program, Department of Geological Sciences, University of Florida, Gainesville, Florida 32611, USA

Eugene Domack
Department of Geosciences, Hamilton College, Clinton, New York 13323, USA

Heather Schrum
Department of Geosciences, Hamilton College, Clinton, New York, USA

Now at Graduate Program in Biological Oceanography, Graduate School of Oceanography, University of Rhode Island, Narragansett, Rhode Island 02882, USA

Albert Benthien
National Ocean Sciences Accelerator Mass Spectrometer Facility, Woods Hole Oceanographic Institution, Woods Hole, Massachusetts, USA

Now at Department of Biosciences/Biogeosciences, Alfred Wegener Institute, D-27570 Bremerhaven, Germany

John M. Hayes
National Ocean Sciences Accelerator Mass Spectrometer Facility, Woods Hole Oceanographic Institution, Woods Hole, Massachusetts 02543, USA

[1] We report a detailed programmed-temperature pyrolysis/combustion methodology for radiocarbon (^{14}C) dating of Antarctic sub-ice shelf sediments. The method targets the autochthonous organic component in sediments that contain a distribution of acid-insoluble organic components from several sources of different ages. The approach has improved sediment chronology in organic-rich sediments proximal to Antarctic ice shelves by yielding maximum age constraints significantly younger than bulk radiocarbon dates from the same sediment horizons. The method proves adequate in determining isotope ratios of the pre-aged carbon end-member; however, the isotopic compositions of the low-temperature measurements indicate that no samples completely avoided mixing with some proportion of pre-aged organic material. Dating the unresolved but desired young end-member must rely on indirect methods, but a simple mixing model cannot be developed without knowledge of the sedimentation rate or comparable constraints. A mathematical approach allowing for multiple mixing components yields a maximum

likelihood age, a first-order approximation of the relative proportion of the autochthonous component, and the temperature at which allochthonous carbon begins to volatilize and mix with the autochthonous component. It is likely that our estimation of the cutoff temperature will be improved with knowledge of the pyrolysis kinetics of the major components. Chronology is improved relative to bulk acid-insoluble organic material ages from nine temperature interval dates down to two, but incorporation of inherently more pre-aged carbon in the first division becomes more apparent with fewer and larger temperature intervals.

Components: 8190 words, 10 figures, 3 tables.

Keywords: Antarctica; sediment chronology; radiocarbon; pyrolysis; sedimentary organic material; carbon isotopes.

Index Terms: 1115 Geochronology: Radioisotope geochronology; 1125 Geochronology: Chemical and biological geochronology; 0728 Cryosphere: Ice shelves.

Received 5 September 2007; **Revised** 15 January 2008; **Accepted** 28 January 2008; **Published** 2 April 2008.

Rosenheim, B. E., M. B. Day, E. Domack, H. Schrum, A. Benthien, and J. M. Hayes (2008), Antarctic sediment chronology by programmed-temperature pyrolysis: Methodology and data treatment, *Geochem. Geophys. Geosyst.*, *9*, Q04005, doi:10.1029/2007GC001816.

1. Introduction

[2] When datable carbonate minerals are absent, the use of sedimentary, acid-insoluble organic material (AIOM) for sediment core chronology is necessary. Bulk radiocarbon dating of AIOM is normally applied in such cases [*Andrews et al.*, 1999; *DeMaster et al.*, 1996; *Domack et al.*, 2001; *Kellogg et al.*, 1979; *Licht et al.*, 1996, 1998], but becomes ambiguous when allochthonous carbon derived from multiple sources of different ages is present [*McGeehin et al.*, 2001, 2004]. Biased ages resulting from the simultaneous immobilization of pre-aged carbon and fresh carbon in a sediment horizon have been well documented in Antarctic sediments from both the Ross Sea and near the Palmer Peninsula [*Andrews et al.*, 1999; *Domack*, 1999]. In both locations, radiocarbon chronologies have necessitated surface ages well in excess of the accepted 1.2 ka reservoir age to explain core top ages [*Andrews et al.*, 1999; *DeMaster et al.*, 1996; *Domack*, 1999]. An improvement to the bulk radiocarbon technique for such sediments is imperative for comparisons between ice core climate records and sedimentary records of ice shelf collapse [*Andrews et al.*, 1999].

[3] Several methods have been conceived to improve bulk radiocarbon dates where ambiguities related to mixing of carbon sources exist. Elegant methods such as compound-class and compound-specific radiocarbon dating [*Eglinton et al.*, 1996], which have been successfully applied elsewhere in the Antarctic [*Ohkouchi*, 2003; *Ohkouchi and Eglinton*, 2006], are limited in Antarctic peninsula sediments due to low concentrations of desirable compound classes such as sterols relative to pre-aged carbon [*Villinski et al.*, 2008].

[4] We have approached the dating of AIOM in Antarctic sediments by exploiting the difference in thermochemical stability between fresh autochthonous AIOM and diagenetically stabilized allochthonous AIOM. The result has been improvement of the chronologies by establishment of a maximum age constraint, significantly younger than bulk radiocarbon ages, on individual sediment horizons. Here we provide a detailed description of a flow-through incremental programmed-temperature pyrolysis method, focusing on the considerations necessary to provide minimum age constraints and maximum likelihood ages required for correlation of sedimentary ice shelf records to high-resolution climate records such as those interpreted from ice cores. The following discussion will focus on a sample that was analyzed at very high resolution to demonstrate proof of concept, as a well as a lower-resolution treatment of a core possessing radiocarbon-dated foraminifer tests.

2. Methods

[5] Sediments from two kasten cores (KC-49 and KC-5) taken from 600 and 400 m.b.s.l. aboard the *Nathaniel B. Palmer* in 2001 (Figure 1) were sampled and dried shipboard as previously described [*Domack et al.*, 2001]. At the National Ocean Sciences Accelerator Mass Spectrometer

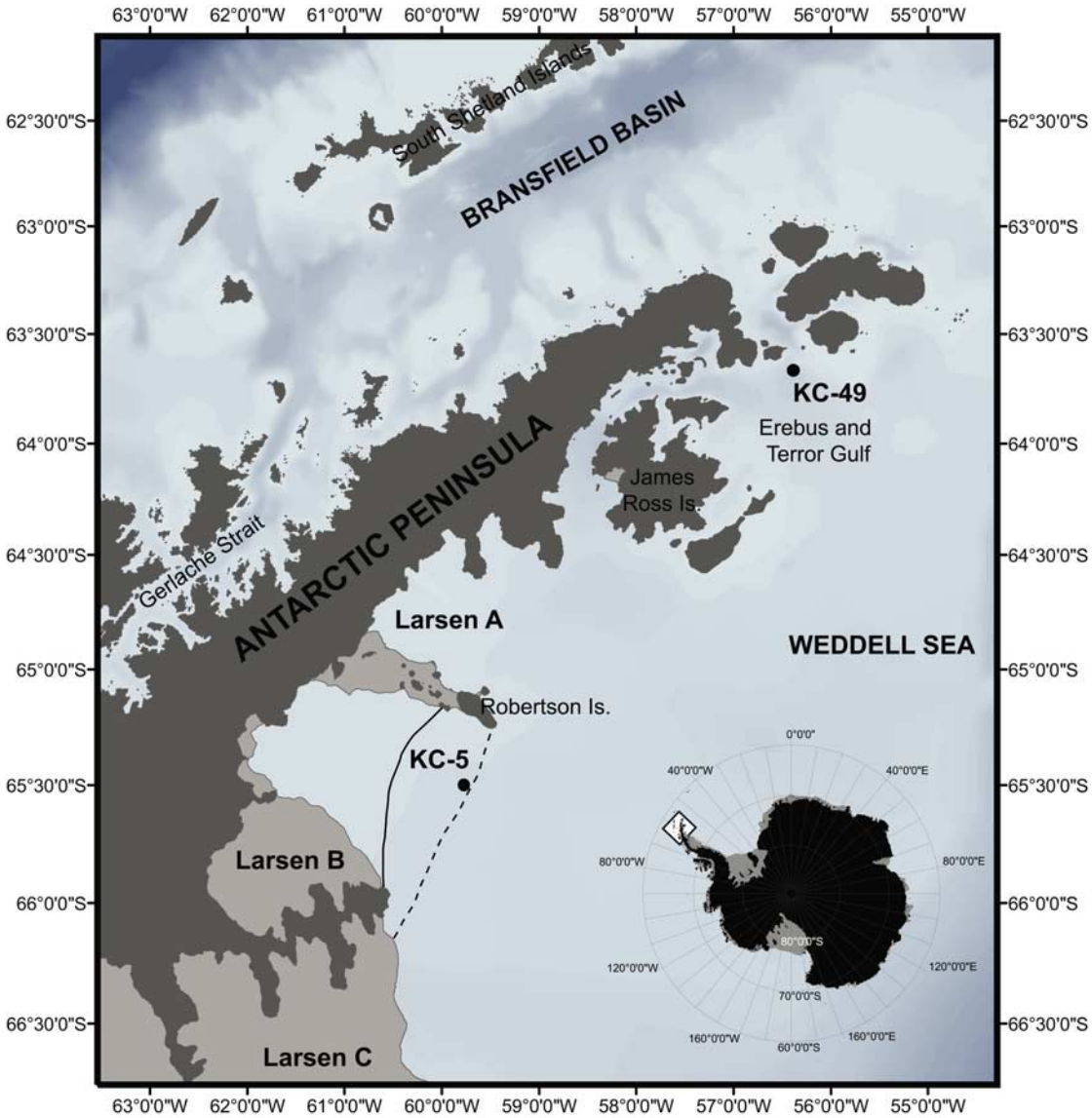

Figure 1. Location of cores analyzed from NW Weddell Sea, Antarctica. Extent of Larsen Ice Shelf B is shown by the dashed line (pre-2002) and the solid line (post-2002 collapse). Kasten core 5 is located at the most recent extreme of the ice shelf.

facility (NOSAMS, Woods Hole Oceanographic Institution), the samples were rinsed with 10% HCl at room temperature for 60 minutes to dissolve carbonates while minimizing hydrolysis of organic material. Samples were dried in a low-temperature oven for 24 h. Aliquots of 0.1–0.3 g dried sediment were weighed onto quartz wool (pre-combusted in air for 2 h at 525°C) in a quartz flow-through reactor (Figure 2).

[6] The quartz reactor was supported within the top portion of a quartz combustion chamber (Figure 2) at the axis of a tube furnace. Both the quartz reactor and the combustion chamber were cleaned by baking at 850°C. The annular space between the quartz vessels was continuously purged with ~5 mL/min of ultra-high-purity (UHP) O_2 in He, while the central reaction vessel was continuously purged with 30 mL/min of UHP He (Figure 2). These rates were chosen to rapidly transfer pyrolysis products to the combustion chamber, to prevent back-streaming of O_2 into the pyrolysis reactor, to provide adequate contact times in the combustion chamber, and to purge the CO_2 detector rapidly enough to provide good dynamic response to varying releases of carbon. The pyrolysis furnace was programmed to provide a gradual temperature ramp of +5°C/min. Just below the sample chamber, the annular and axial gas streams mixed, adding O_2

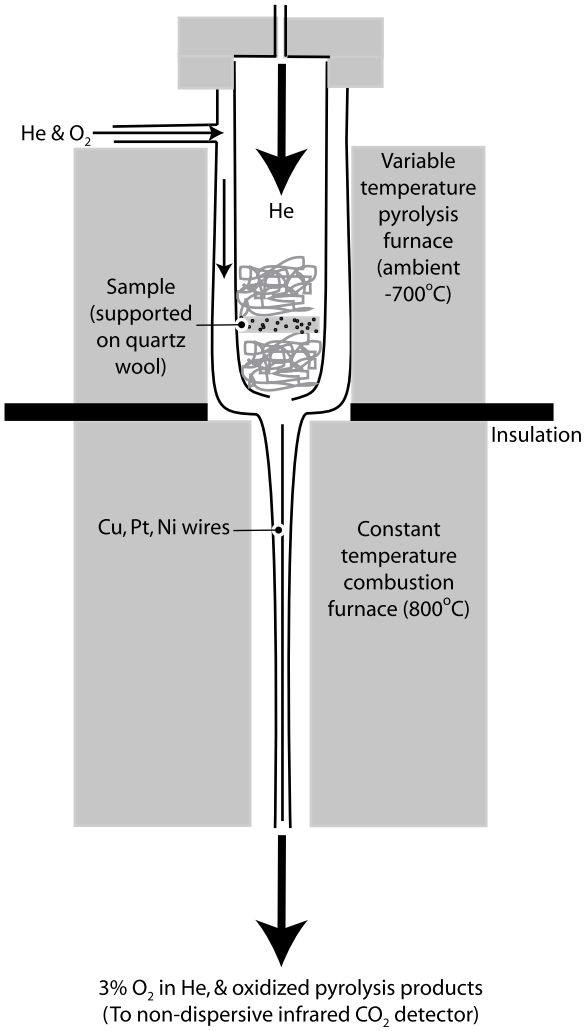

Figure 2. Schematic diagram of pyrolysis reactor.

to the stream of pyrolysis products entering the quartz combustion chamber. A second tube furnace around this section was set at a constant temperature of 800°C. The gas flowing downstream of the confluence consisted of 3% O_2 together with the pyrolysis products in a balance of He. Oxidized Cu wire intertwined with Pt and Ni wires catalyzed the conversion of pyrolysis products into CO_2.

[7] Directly downstream from the combustion furnace, the sample flowed through a nondispersive infrared CO_2 detector and subsequently to one of two cryogenic traps composed of 8 loops of Pyrex tubing (4 mm o.d., 3 mm i.d.) partially immersed in liquid N_2. The traps were connected to an assembly of six remotely controlled, vacuum-actuated valves. By toggling the valve states, one trap could accumulate condensable products from the gas stream while the other was open to a vacuum line for gas transfer and purification. The photometrically determined CO_2 concentration was recorded with simultaneous temperature readings from the pyrolysis furnace. Integration of the CO_2 signal provided a cumulative molar total of CO_2 that had evolved during pyrolysis of the sediment sample. This total served as a fundamental guide for splitting of optimal sized samples for AMS ^{14}C measurement.

[8] In the vacuum line, gas samples transferred from the trapping system were distilled to remove H_2O and incondensables, and then quantified manometrically. Manometric measurements were conservatively within 10% of photometric measurements, primarily varying due to interfering gases such as water flowing through the CO_2 analyzer. Accuracy of both manometric and photometric quantification of CO_2 was tested periodically using thermal evolution of CO_2 from known quantities of $NaHCO_3$, illustrating improved photometric yields with "clean" CO_2 gas (Figure 3). Yields measured photometrically did not vary significantly over the range of temperatures (5% relative standard deviation (%RSD) between CO_2 pulses (Figure 3)). The observation that both photometric and manometric determinations of the CO_2 evolved from Na_2CO_3 decomposition (second peak) were higher than the measurements of CO_2 evolved from $NaHCO_3$ dehydration (first peak) implies that the $NaHCO_3$ reagent was contaminated with Na_2CO_3. The amount of contamination implied is in the vicinity of 1%. Nonetheless, this exercise afforded periodic verification of both CO_2 quantification methods as well as the accuracy of the thermocouple readings at the point of reaction.

[9] The following results and discussion pertain to three samples from two kasten cores (Figure 1). Kasten core 49 (KC-49) contained three distinct sedimentological units (Figure 4a) which represent the progression from glacial conditions to deglacial (sub-ice shelf) and finally to open marine setting. A muddy diamicton, a granulated unit, and a thick, diatom rich, mud unit, respectively, represent these conditions. The glacially sculpted seafloor (red dotted line in Figure 4c) is in agreement with the presence of a glacial till that forms part of a series of mega-scale glacial lineations found across the Erebus and Terror Gulf [*Camerlenghi et al.*, 2001; *Backman and Domack*, 2003]. This morphology is overlain by a hemipelagic drape and drift deposit (the Vega Drift) [*Camerlenghi et al.*, 2001]. High-resolution seismic data of the Vega Drift (Figure 4c)

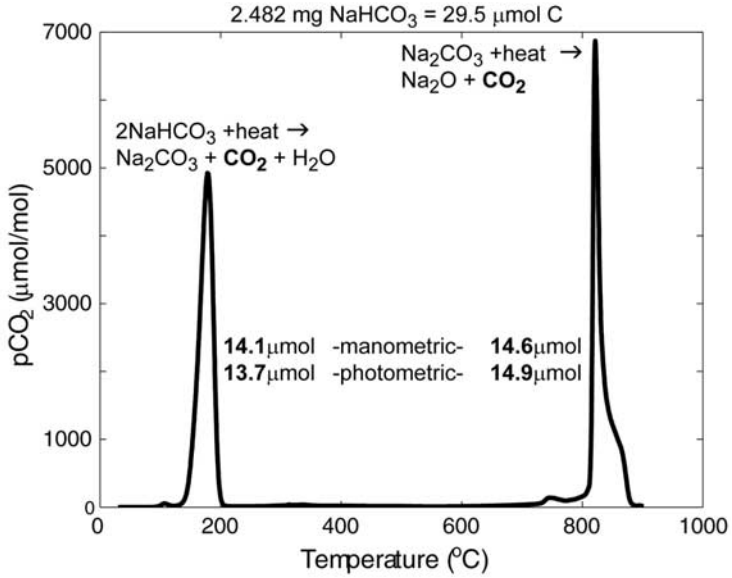

Figure 3. Sodium bicarbonate quantification. The thermal evolution of sodium bicarbonate in a He atmosphere allowed comparison of both methods of CO_2 quantification used in this approach. Yields from both photometric and manometric measurements were 97% of the known quantity. The separate CO_2 peaks were identical to within a 3.5–5.6% relative standard deviation (RSD, manometric-photometric, respectively). This exercise also allowed periodic verification that thermocouple temperature readings were indicative of actual temperatures at the point of reaction. Here, the dehydration of bicarbonate and the decomposition of sodium carbonate occurred near the well-documented temperatures of 180°C and 850°C, respectively. Because both the photometric and manometric determinations of the decomposition peak are similarly larger than the same determinations of the dehydration peak, it is probable that the sodium bicarbonate reagent used contained 1% Na_2CO_3.

were used as a guide to locate an ideal setting for the extraction of core KC-49. Sediment accumulation rates in the coring site were significantly lower than regions to the south, thus the glacial and Holocene marine sediment record is condensed to less than one-fourth the thickness of the sediment drift to the south. Although the second kasten core, KC-5 (Figure 1), also contains three stratigraphic intervals (a diamicton, a gravelly sand to granulated mud, and a sandy mud), none represent open marine conditions. The lower glacial unit transitions to a grounding line facies and then into a subglacial facies [*Domack et al.*, 2005]. Samples from KC-49 (244–245 cm) and KC-5 (1–4 cm and 24–25 cm horizons), each weighing 0.3 g, were pyrolyzed and evolved gas was collected at approximately 12 μmol C intervals (Table 1) resulting in 9 measurable aliquots of CO_2 for KC-49 and at approximately 27 μmol intervals for KC-5 resulting in 2–3 aliquots. Approximately 10% of each of these splits was taken for determination of $\delta^{13}C$ ratios and the balance graphitized by standard Fe-H_2 reduction for measurement using conventional AMS techniques.

[10] Early attempts at this procedure yielded samples with a cloudy condensate visible upon freezing into 6 mm Pyrex tubes and flame sealing under vacuum after manometric measurement. Subsequent samples, including KC-49 244–245, were frozen on copper oxide and granulated silver, and combusted redundantly at 525°C for 2.5 h to ensure complete transition of pyrolysis products to CO_2 and removal of sulfur; both deemed as possible causes for the cloudy residue. Evolved gases that displayed this residue were normally from the lowest-temperature intervals of the pyrolysis sequence (100°C–320°C) and they produced a translucent, yellow refractory residue on the inner wall of the 9 mm Pyrex tubes after redundant combustion. The residue did not affect graphitization yield. To investigate the chemical provenance of the yellow residue, several methods were attempted for qualitative analysis using ICP-MS. Sonication of the tubes containing residue in concentrated nitric acid did not appreciably mobilize the refractory residue. Laser ablation sampling of glass pieces containing this residue was successful in mobilizing some proportion of the residue for

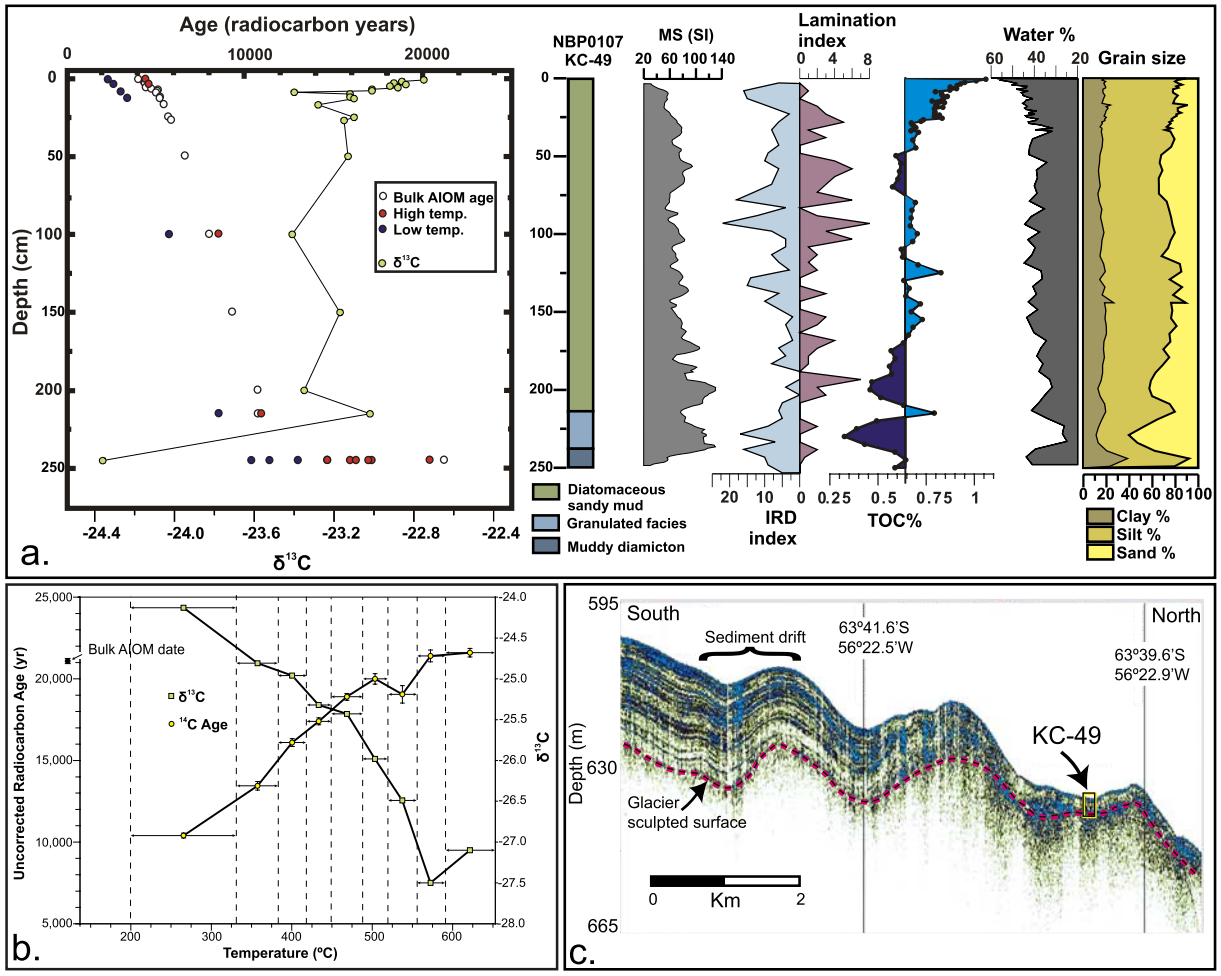

Figure 4. Radiocarbon dates and core stratigraphy for NBP 01-07 KC-49 from the NW Weddell Sea. (a) Stratigraphic fence diagram illustrating bulk AIOM and programmed-temperature pyrolysis radiocarbon dates, $\delta^{13}C$ values, lithofacies, magnetic susceptibility, IRD index, lamination index, TOC, water %, and grain size in KC-49. High- and low-temperature ^{14}C ages were obtained with an earlier version of the pyrolysis system that did not measure CO_2 concentration evolving from the pyrolysis chamber. (b) Programmed-temperature pyrolysis radiocarbon dates and $\delta^{13}C$ for KC-49 244-245 cm (muddy diamicton). CO_2 was collected at higher resolution in the current version of the pyrolysis system to demonstrate the age progression from low- to high-temperature yields. (c) High-resolution (Chirp) seismic profile across the Vega Drift, with location of KC-49 indicated. Diminishing thickness of postglacial sediments from south to north across the Vega Drift is visible. Vertical scale calculated by assuming the velocity through water is 1500 m/s. Relief of glacial sculpted seafloor is indicated by red dotted line.

analysis by ICP-MS. Relative to Pyrex tubes containing copper oxide and "clean CO_2" which were sealed under vacuum and heated to 525°C, the tubes containing the yellow residue displayed copper count rates of 3 orders of magnitude higher. Chloride could not be measured using this technique, but it is likely that the residue was an insoluble complex of copper chloride.

3. Results

[11] Original bulk AIOM ages for KC-49 (Figure 4a) increase in a smooth curve down core through the diatomaceous mud and granulated units, but the date from the diamicton facies lies well out of this progression. A preliminary version of the pyrolysis which did not actively measure CO_2 in-line (thus inhibiting the ability to carefully resolve a targeted aliquot of gas) was applied to seven sediment samples from KC-49 in duplicate of the bulk-dated horizons. Dates based on organic C released at high temperatures (red points in Figure 4a) are consistently similar to the original bulk AIOM dates. In the diatomaceous mud and granulated facies, those based on organic C released at low temperatures (blue points in Figure 4a) are 2000–3000 years

Table 1. Pyrolysis and Isotope Data for Each Temperature Interval[a]

Interval	CO_2, μmol	T_{min}, °C	T_{max}, °C	f_M (1σ)	$\delta^{13}C$, ‰ VPDB	Age, ^{14}C years (1σ)
1	11.5	ambient	320	0.2746 (0.0052)	−24.1	10400 (150)
2	13.5	320	375	0.1872 (0.0062)	−24.8	13450 (260)
3	12.8	375	410	0.1348 (0.0040)	−25.0	16100 (240)
4	17.3	410	450	0.1145 (0.0030)	−25.3	17400 (210)
5	21.4	450	485	0.0951 (0.0025)	−25.4	18900 (210)
6	20.5	485	520	0.0831 (0.0033)	−26.0	20000 (320)
7	21.9	520	555	0.0936 (0.0062)	−26.5	19050 (570)
8	15.8	555	595	0.0700 (0.0032)	−27.5	21400 (360)
9	11.6	595	685	0.0976 (0.0022)	−27.1	21600 (260)

[a] The amount of CO_2, quantified manometrically, corresponds to the temperature range constrained by T_{min} and T_{max}. The fractions modern shown are corrected for $\delta^{13}C$, and age is calculated using the Libby half-life of ^{14}C. Either the $\delta^{13}C$ column or the f_M column (if uncorrected for $\delta^{13}C$) can be substituted into equation (1) as the vector **A**.

younger. In the diamicton unit, low-temperature dates were over 10,000 years younger than the bulk AIOM dates. The contrast between the high- and low-temperature ages indicates that reworked organic carbon is released mainly at high temperatures. That much larger difference between the high- and low-temperature ages in the diamicton indicates a greater influence of reworked carbon in that unit. The effect is notably stronger in the diamicton, as indicated by the large difference in the $\delta^{13}C$ values between the diamicton and the rest of the core.

[12] Heating of the sample to 700°C in a He atmosphere was sufficient to quantitatively convert all organic matter to CO_2. The total CO_2 evolved from the pyrolysis of KC-49 244–245 (Figure 5), normalized to the weight of the sample analyzed, reflects a 0.57% OC content which compares well to LECO-measured values of 0.55%–0.63% total carbon quantified at temperatures of 900°C (Figure 4a). In the worst-case scenario that the low-temperature fraction residues were copper complexed with an organo-acid derivative of the pyrolysis products that did not completely oxidize, they represent an insignificant amount of the total carbon evolved in the low-temperature fractions based on the agreement between our quantification of %C and determination of the same quantity by the LECO technique.

[13] Radiocarbon ages and photometric CO_2 concentrations from KC-49 are shown relative to temperature in Figure 5. Ages of individual temperature fractions ranged from 10,400 years (f_M = 0.274) to 21,600 years (f_M = 0.068) (Table 1),

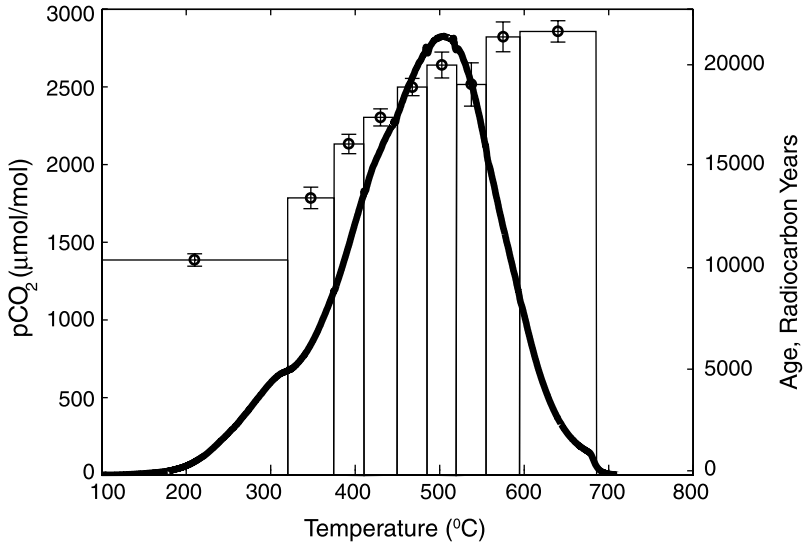

Figure 5. KC-49 thermograph. The heavy black line corresponds to pCO_2 (photometric) on the left axis as a function of temperature. The bars represent the temperature range over which a sample was trapped (width) and the age in radiocarbon years of that sample (height, right axis). Uncertainty on the radiocarbon ages is plotted as ±1σ.

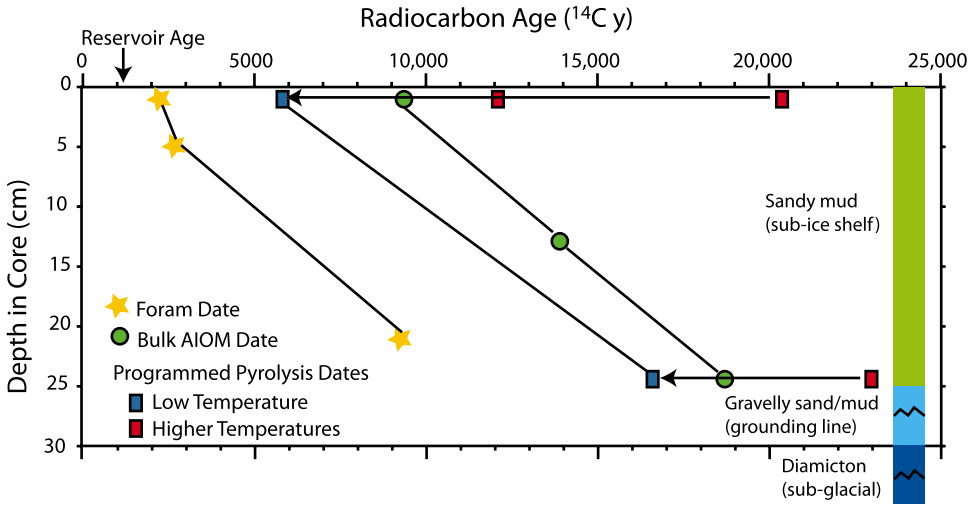

Figure 6. Pyrolysis ages from KC-5. Less finely divided sampling of the pyrolysis products than in core KC-49 produced significant improvement over bulk AIOM ages; however, the low-temperature component did not match the foramifer ages from the same horizons. This is due to the increased mixing of pre-aged carbon with the autochthonous component during the increased temperature domain over which the first split was taken.

compared to a bulk age of 21,000 years. The ages of individual temperature fractions increased nearly monotonically with temperature. Stable isotopic compositions of the evolved CO_2 decreased from −24.1‰ to −27.5‰ VPDB with higher temperatures, until increasing by 0.5‰ in the last temperature fraction (Figure 4b). In terms of both measured carbon isotope ratios, there was a marked decrease in the rate of change between the final two temperature fractions, and the ages of these fractions are analytically indistinguishable.

[14] Radiocarbon ages from pyrolysis fractions, bulk AIOM, and forams in KC-5 are shown in Figure 6. Again, pyrolysis ages increased monotonically with temperature and improved upon old-biased bulk AIOM ages. The pyrolysis ages, sampled at a less rigorous resolution than KC-49 244–245 cm, approach but do not match foraminifer ages.

4. Discussion

4.1. Assessing the Magnitude of Chronological Improvement

[15] Ideally, a sediment core would possess either easily datable foram tests or enough fresh organic material to separate specific compounds at an adequate yield for radiocarbon dating. Near KC-49, at the low-latitude reaches of the Antarctic Peninsula, the latter seemed a viable option in terms of the amount of organic material. Dates from specific compounds as well as compound classes proved to be highly ambiguous indicating significant reworking of the sediment and mixing of organic material of different ages [*Ohkouchi et al.*, 2000]. In the sub-ice shelf sediments of KC-5, fresh sterols were not extractable from any horizon below the surface sediments due to both low productivity below the ice shelf and dilution of organic material by diagenetically altered material [*Roe et al.*, 2006]. In both cases, reworked organic material has likely attained a higher degree of diagenetic stability, yielding leverage by which fresh organic material could be isolated and dated.

[16] The aim of this experiment was to release fresher material first. Neither combustion nor pyrolysis is perfect in this regard. Pyrolysis was chosen as preferable because it is less purely a chemical distinction. Fresh organic debris was expected to yield more volatile products than diagenetically altered organic material. The results in Figures 4–6 illustrate success in separating, to a first order, components of different ages.

[17] The results in Figures 4–6 also indicate the significant improvement in chronology achieved by this method. Despite the improvement, the results show that the actual ages of these sediment horizons, while better constrained, remain unknown (KC-49) or unresolved (KC-5). Pyrolysis of $NaHCO_3$ illustrates an ideal situation where the pyrolysis products of carbon sources (one source from dehydration of $NaHCO_3$ at ~180°C, and another from decomposition of Na_2CO_3 at ~850°C) with different thermal stabilities are well

separated and easily differentiable (Figure 3). It is unrealistic to expect such an ideal resolution of carbon components when dealing with multiple sources of organic material. Instead, an optimistic expectation for our approach would be the resolution of a low-temperature age plateau. The significant differences between low-temperature ages in KC-49 244–245 (i.e., the lack of a low-temperature age plateau) indicate that even the lowest-temperature fraction contains at least some older, allochthonous material, and the proportion of this material increases from a value greater than zero in the lowest-temperature fraction. Greater mixing of pre-aged carbon into the first temperature interval would be expected of less finely resolved KC-5. Thus the youngest age from this approach represents a maximum age constraint for the autochthonous material in this particular core horizon, and it is likely that the actual age of autochthonous material may be younger. In order to apply this method to compare sedimentary records to high-resolution paleoclimate archives, a means to estimate the maximum likelihood ages of the autochthonous carbon fraction must be established.

[18] A two-point mixing model with both an autochthonous and an allochthonous end-member would be desirable; however, neither core lends enough clues for success with such a simplified approach. Figures 4b and 5 illustrate that the method confidently determines the isotope ratios of the allochthonous end-member in KC-49 244–245 cm (i.e., there is a high-temperature age plateau), with a $\delta^{13}C$ ratio of $-26.8 \pm 0.6‰$ and a f_M of 0.079 ± 0.012 calculated from the averages and standard deviations of the final four temperature intervals. In the absence of either a complementary low-temperature plateau or knowledge of the mixture proportions, however, a mixing model cannot be constructed. If ages were known with better confidence either up-core or down core as in KC-5, an extrapolation could be made to 244–245 cm and used to estimate the absolute age of the young AIOM and, subsequently, the proportion of older material present. Although sediment deposited in diatomaceous horizons above 244–245 cm in the core may yield higher proportions of autochthonous organic material, the sediment core KC-49 contains no horizons with datable material other than AIOM, rendering this approach to establishing a mixing model unwieldy. The situation in KC-5 is not much improved despite knowledge of foraminifer ages. Here, the subsampling of pyrolysis products was not of high enough resolution to estimate either a pre-aged or autochthonous end-member. Furthermore, in presence of differential deposition [*Mollenhauer et al.*, 2005] and bioturbation relative to particle size [*Bard*, 2001], the question of the true age of AIOM would remain in spite of a foramifer age.

4.2. An Objective Estimate of the Autochthonous Component

[19] Without the necessary information for construction of a simple mixing model, an independent method by which ages, isotope ratios, and relative contributions of AIOM components can be conceived using only the structure of the thermograph in Figure 5. Even in the absence of discrete peaks such as those provided by $NaHCO_3$ (Figure 3), the KC-49 thermograph demonstrates the presence of multiple components simply in terms of variations in the radiocarbon and stable isotopic compositions of individual temperature fractions. In absence of the low-temperature plateau, two inflection points on the rising limb of the thermograph can be conceived to signify changes in proportions of young, intermediate, and old sources of carbon. An estimation of the amounts of these components can be used to approach the maximum likelihood age and the relative proportion of the young AIOM component with an assumption about the pyrolysis kinetics of the individual AIOM components.

[20] In similar stable isotopic measurements of pyrolysis products, a Gaussian distribution of pyrolysis activation energies constituted a workable first-order approximation where the pyrolysis kinetics of the chemical classes present within the substrate were not precisely known [*Cramer*, 2004]. The thermograph of KC-49 244–245 (Figure 5) can be decomposed into three Gaussian curves using a nonlinear regression procedure (Figure 7). An attempt to decompose the thermograph into four Gaussian curves resulted in an increase in iterations of the model from 18 to 111, which supports the significance of the inflection points suggested by the structure of the thermograph and illustrates the futility of trying to discern minor components (components that are small enough to not cause thermograph inflection points) despite the likelihood of their presence. Although several local minimizations exist, the two most plausible solution sets are shown in Table 2.

[21] With three significant components of unknown age and $\delta^{13}C$, the nine measurements of

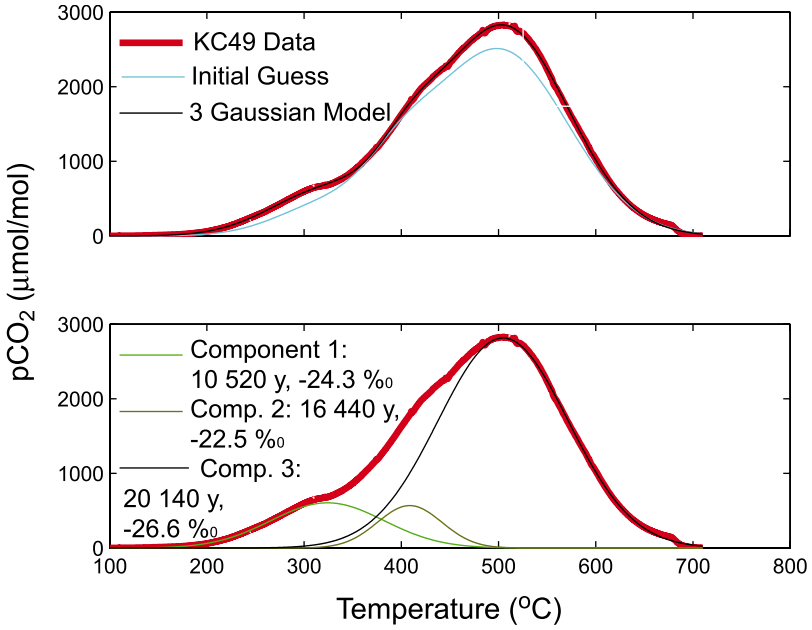

Figure 7. Gaussian decomposition of KC-49 thermograph. A nonlinear least squares technique was used to decompose the thermograph (heavy red line in both panels) into reaction components, assuming Gaussian distribution of pyrolysis activation energies. To apply this technique, a first guess must be made (cyan line, top panel) to initiate an iterative process to minimize the model residuals. The result (black line, top panel) displays good fit and represents the absolute minimum residual of several solutions. The individual components of this model are shown with the calculated isotope ratios of each one (bottom panel).

these quantities can be used to describe an overdetermined system of linear equations:

$$\begin{bmatrix} A_1^M \\ A_2^M \\ : \\ A_i^M \end{bmatrix} = \begin{bmatrix} f_{1,1} & f_{1,2} & .. & f_{1,j} \\ f_{2,1} & .. & .. & : \\ : & .. & .. & : \\ f_{i,1} & .. & .. & f_{i,j} \end{bmatrix} \times \begin{bmatrix} A_1^C & A_2^C & .. & A_j^C \end{bmatrix}, \quad (1)$$

where superscripts M and C refer to measurements and significant components, respectively. In this case, i is the number of measurements and j is the number of components. Vectors [**A**] can be either fractions modern of radiocarbon (uncorrected for $\delta^{13}C$) or stable isotope compositions, with the component fraction matrix [***f***] determined by the nonlinear regression of Gaussian solutions to the thermograph with the minimum residual summed between temperature divisions used during the experiment. To account for all CO_2 evolved during each ith temperature interval of each pyrolysis, we use the equality,

$$\sum_{n=1}^{j} f_{i,n} = 1, \quad (2)$$

whereby each ith row of the component fraction matrix [***f***] must sum to 1.

[22] Radiocarbon solutions of equation (1) for the proportions in Table 3 must be constrained to prevent negative fractions modern. Further, fractions modern uncorrected for stable isotope composition are used in vector [$\mathbf{A^M}$], but fractions

Table 2. Gaussian Parameters of Plausible Solution Sets to the Nonlinear Regression of the Thermograph Data[a]

	Solution	
	1	2
Component 1		
Height, µmol/mol	606	308
Center, °C	324	286
Width, °C	82	57
Component 2		
Height, µmol/mol	569	2296
Center, °C	409	473
Width, °C	47	120
Component 3		
Height, µmol/mol	2814	805
Center, °C	505	532
Width, °C	95	64
RMSR	14.32	21.73

[a] Solution set 1 is taken as the more applicable of the two sets because it has a lesser root mean square of the residuals, and when applied to solving equation (1), it does not run against the physical constraints of $f_M > 0$.

Table 3. Component Proportions of Gaussian Decomposition, Solution 1[a]

	Component		
Interval	1	2	3
1	0.96	0.00	0.03
2	0.62	0.15	0.23
3	0.20	0.33	0.47
4	0.06	0.21	0.73
5	0.01	0.05	0.94
6	0.00	0.01	0.99
7	0.00	0.00	1.00
8	0.00	0.00	1.00
9	0.00	0.00	1.00
Total	0.16	0.08	0.76

[a] These proportions are defined for each interval as the area under the given component in Figure 5. The proportions make up the matrix f in equation (1), and the sum of each components proportions indicates the relative amount of autochthonous carbon to pre-aged carbon of different sources.

modern are re-corrected to specific component $\delta^{13}C$ values from vector $[\mathbf{A}^{\mathbf{C}}]$ after equation (1) has been solved for both isotopes measured. No constraints were applied to the stable isotope solutions to the system. For both the radiocarbon and $\delta^{13}C$ systems, a constrained nonlinear routine was employed, with initial guesses similar to the simple algebraic solutions. Equation (1) was solved for $[\boldsymbol{f}]$ constructed from two plausible Gaussian regression solution sets (Table 2) despite one set producing a significantly lower residual. The solution of equation (1) using Gaussian regression 2 (Table 2) includes a component with $f_M < 0$, rendering it unstable and confirming the lesser root mean square of the residuals of solution 1 as an indicator of the most realistic solution.

[23] At an age of 10,520 years, the youngest component in the solution to equation (1) is indistinguishable from the maximum age constraint provided by direct measurement of the low-temperature pyrolysis age. All of the stable isotope values in the $\delta^{13}C$ solution set are within published measurements on compound class carbon isotopic values from nearby Antarctic seas [*Ohkouchi and Eglinton*, 2006]. The model is consistent, but how accurate is this objective estimate of the actual age and proportion of autochthonous material at this core depth in KC-49? The answer lies in the assumptions about reaction kinetics for the pyrolysis of sedimentary organic material from the east coast of the Antarctica Peninsula. It is prudent, therefore, to constrain the autochthonous age with an independent approach for comparison in absence of knowledge of the exact reaction kinetics.

[24] Comparing end-member characteristics with inverse cumulative yield normally results in a linear relationship if the model is of simple mixing. Assuming the amount of autochthonous carbon is negligible in the temperature intervals after the first, this relationship (Figure 8) can provide further constraint on the age of the autochthonous component. The slope of this linear relationship (b) is related to the autochthonous age (expressed here as $\Delta^{14}C$) by

$$b = N_s\left(\Delta^{14}C_s - \Delta^{14}C_t\right), \tag{3}$$

where subscripts s and t refer to autochthonous and allochthonous components, respectively, and N is the number of micromoles of carbon in the lowest-temperature interval, assuming that only negligible amounts of the autochthonous component were present in temperature intervals 2–9 and that the final four intervals are representative of the pre-aged end-member. In other words, the age difference between the autochthonous component and the oldest allochthonous carbon is related to the slope of the linear relationship in Figure 8, in proportion to the amount of autochthonous material in the lowest-temperature interval. Given information about the age of the allochthonous component and the proportion of autochthonous component in the lowest-temperature interval, an additional age constraint on the autochthonous component can be derived. Again, Figure 5 illustrates that a fair estimate of the allochthonous fraction is provided by the final four temperature intervals ($f_M = 0.079 \pm 0.012$). Further, the Gaussian decomposition approach allows a viable estimate of the fraction of autochthonous material in the first temperature fraction (0.96, Table 3); however, it does not provide a straightforward uncertainty (the largest uncertainty is likely the model selection, in any case). If the first temperature interval was entirely autochthonous carbon, these values would yield an age of 9650 ± 330 ^{14}C years. This age decreases to 9020 ± 300 ^{14}C years if it is assumed that the lowest-temperature interval consisted of only 90% autochthonous carbon. Such a range in compositions is not entirely out of the question, especially in the case where our assumption of Gaussian reaction kinetics is not accurate. The range in ages of these scenarios varies from the maximum likelihood Gaussian component age of 10,520 ^{14}C years by significantly more than the analytical uncertainties of radiocarbon dates in this

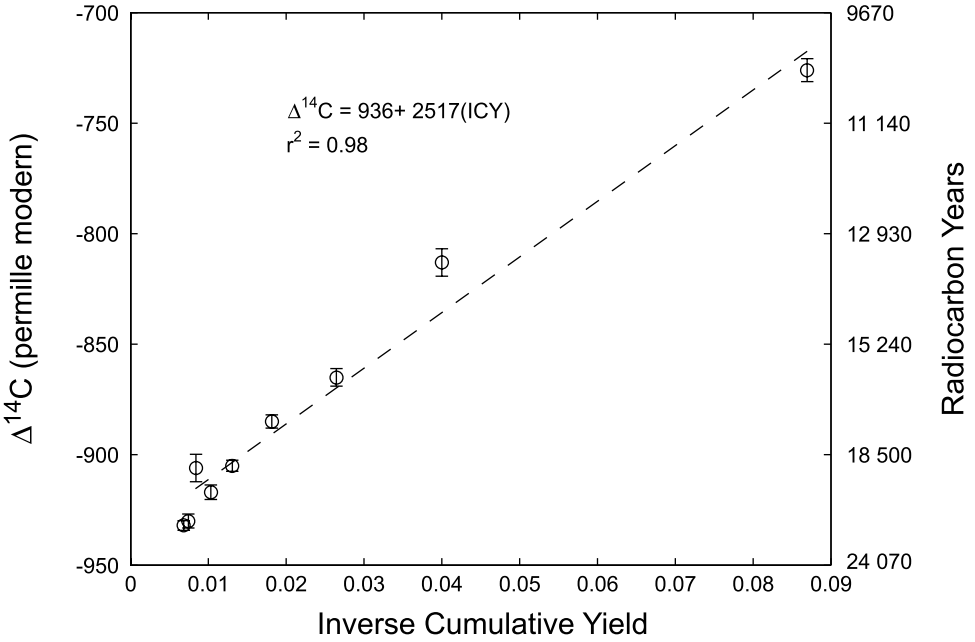

Figure 8. Inverse cumulative yield plot of $\Delta^{14}C$ measurements. A linear relationship between the inverse cumulative yield and the $\Delta^{14}C$ values measured for each temperature interval provides an independent maximum age constraint for the autochthonous AIOM. Following equation (3), this approach constrains the age of the autochthonous component between 9320 and 9980 ^{14}C years, assuming that the first temperature interval is entirely autochthonous carbon. Assuming a proportion less than 1 decreases this constraint. This constraint is comparable to the maximum likelihood age of 10,520 ^{14}C years from the Gaussian decomposition method, especially in light of the large differences between these ages and the bulk AIOM age.

age range. Still, the difference between these maximum likelihood ages is much less than the difference between bulk dates and the maximum age constraint directly measured from the low-temperature fraction.

[25] The KC-5 sub-ice shelf core provides an additional test of the pyrolysis method against known ages from foraminifer tests in each horizon. Figure 9 shows a Gaussian decomposition for both horizons using the same initial guess. The resulting four Gaussian distributions of major components does well to fit the thermograph of this core which is significantly more descriptive in both horizons than the analyzed horizon of KC-49. Gaussian components from each horizon in KC-5 are centered on the same temperatures indicating a geochemical significance of the components. Unfortunately, only 2–3 actual measurements were made on these horizons rendering the system of equations (equation (1)) underdetermined ($i < j$). This has two consequences. First, equation (1) cannot be explicitly solved for either isotope measurement. Second the inverse yield mixing model discussed above would be in violation of its assumptions of no mixing in the first temperature interval due to the higher temperature defining that interval. This is not to say that every one radiocarbon date must become nine to employ this method; rather enough measurements need to be made to equal or be greater than the amount of major components and at least one sample must come from at or near the cutoff temperature where pre-aged carbon begins to volatilize to alleviate the two consequences, respectively.

4.3. Improving the Method

[26] Evaluation of these two mathematical approaches relative to each other aids in determining which one is more accurate; however, the question is immaterial in comparison to the difference between these age estimations and the bulk AIOM age. The Gaussian approach relays a maximum likelihood age estimation, which is as likely as the assumption of Gaussian pyrolysis activation energies. The linear model approach yields another maximum age constraint which is lower than this maximum likelihood age. The linear mixing model approach makes the assumption of two components in the mixture with negligible amounts of the low-temperature component in subsequent intervals. Conceptually this is favorable, and the Gaussian approach supports the second assumption with

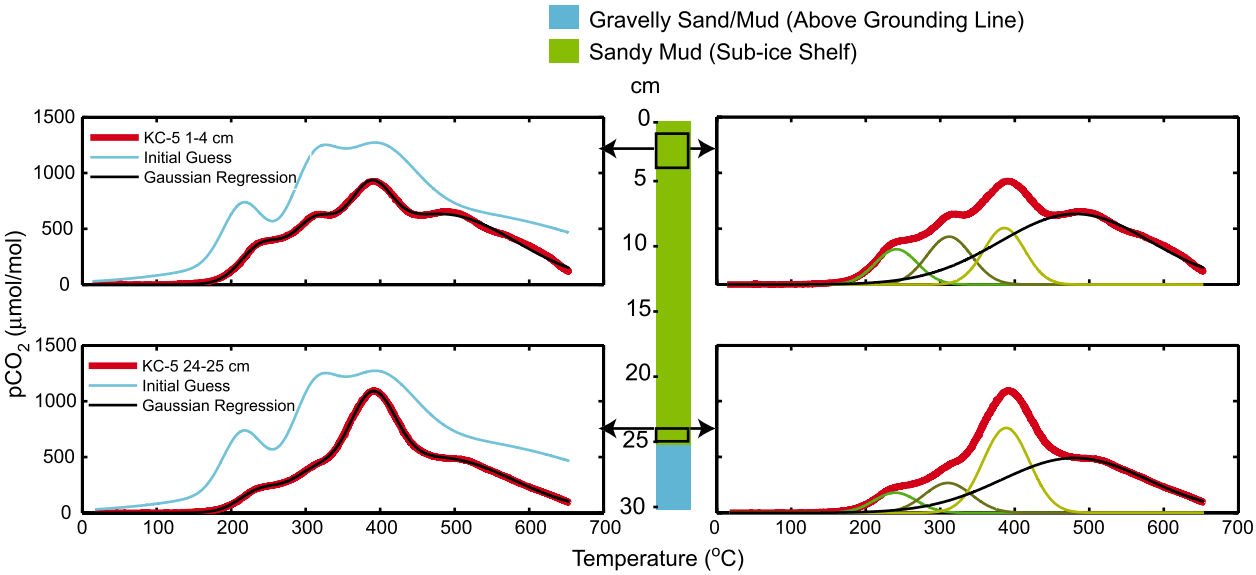

Figure 9. Gaussian decompositions of the KC-5 thermographs. Using the initial guess (blue curves, left side), a nonlinear Gaussian regression (black curves, left side) reproduces the raw data (thick red curves, both sides) very well. Major components brought forth by this analysis (individual Gaussians on right side) are centered at the same temperatures despite being from different core horizons. This implies a geochemical significance to the assumption of Gaussian reaction distributions. The thermographs from KC-5 are more descriptive than KC-49 244-245 cm, and they warrant 4 major components. Because only 2-3 measurements were made on each KC-5 horizon, these systems are underdetermined (after equation (1)) and the maximum likelihood ages of each of the individual components could not be calculated.

only 4% of the autochthonous component being distributed over the remaining 8 temperature intervals. However, the Gaussian approach strongly suggests a third major component which depicts reality more complex than the two component linear model. The difference between these two estimates, however insignificant relative to our assumptions and the bulk age, illustrates that more must be understood about the pyrolysis reactions, but it is not large enough to discredit the significant improvement in chronology offered by this analytical method. Furthermore, improvement of the method is tangible.

[27] Analytically, sampling resolution is ultimately limited by sample size. Our effort to choose a target sample size of 12 μmol C in the proof of concept experiment (KC-49) minimized counting error on AMS analysis of small samples while maximizing the amount of temperature bins analyzed. Sampling at shorter temperature intervals than this is certainly possible but involves a proportional decrease in precision. Short of establishing a maximum likelihood age from the nine radiocarbon measurements, the Gaussian decomposition of the thermograph provides a first-order estimate of the low-temperature cutoff point at which allochthonous C becomes mixed with the youngest major component (Figures 4 and 9). The amount of CO_2 evolved from KC-49 before this temperature (250°C) is approximately 5 μmol (a small but measurable amount), whereas the next 60°C resulted in an additional 7 μmol C.

[28] Sampling at a higher resolution in the temperature domain without sacrificing AMS measurement precision of robust small samples (>10 μmol C) would be ideal. Simply increasing the amount of sediment loaded into the reactor does not seem a viable option. Larger sediment weights either carry enough thermal inertia even during exceedingly slow temperature ramps and/or are volumetrically large enough to be differentially heated by thermal heterogeneities within the furnace to blur the resolution between components. This was observed by the lack of return to baseline levels of CO_2 evolution measured photometrically, even at temperatures as high as 1000°C for several tens of minutes, during pyrolysis of larger samples (~0.5 g). Without increasing sample size, the mathematical approach laid out above illustrates that it is likely that we can analyze a nearly pristine sample of autochthonous C, with some sacrifice in precision on a 5 μmol sample. Attempts to observe any low-temperature plateau in multiple aliquots of the first 5 μmol for an unequivocal estimate of this age is unlikely due to the higher

statistical counting error associated with sample sizes less than 5 μmol. Of course, our estimation of 275°C as the temperature at which mixing of predated C begins to happen during pyrolysis would benefit greatly from a critical assessment of the assumption of Gaussian pyrolysis activation energies of the components.

4.4. Differential Deposition and Bioturbation

[29] Our data corroborate a number of recent reports [*Mollenhauer and Eglinton*, 2007; *Mollenhauer et al.*, 2005, 2006; *Villinski et al.*, 2008] demonstrating that sediment being immobilized at the bottom of the infaunal mixing zone at a given time can have disparate age distributions. Several studies have focused both on the roles of differential bioturbation [*Bard*, 2001] and differential deposition [*Mollenhauer et al.*, 2003, 2005] in producing varying age distributions of different particle classes (e.g., forams versus alkenones) in the same sediment core horizon. In these reports, age differences within a sediment horizon vary up to 4500 years [*Mollenhauer et al.*, 2005]. In addition, *Mollenhauer and Eglinton* [2007] have presented a conceptual model with differential degradation of organic components as cause for large differences in Δ^{14}C. Our resolution of different AIOM components for radiocarbon dating demonstrates age differences between components (~10,000 years) that significantly exceed typical infaunal mixing increments. This poses the question of how the age distributions of differently aged, contemporaneously immobilized sediment components change under the actions of bioturbating infauna. Since the first published work concerning bioturbation [*Darwin*, 1881], the reigning assumption has been of uniform sediment age distributions at the time of deposition into the infaunal mixing horizon. Questions of individual sediment components with different ages have not normally been considered.

[30] Figure 10 shows a series of scenarios involving sediment deposited with different components having age distributions and component proportions similar to those in core KC-49, 244–245 cm (Figure 7 and Table 3). The homogenized increment of sediment represents an amount of time,

$$T_m = \frac{m}{r_d}, \tag{4}$$

where m is the depth of the homogeneous, or bioturbated, layer and r_d is the increment of sediment deposited in a unit time (r_d = dL/dT based on the formulation of *Berger and Heath* [1968], where dL is the thickness of sediment deposited per unit time, dT). Varying this ratio varies the magnitude of the bioturbation footprint on the original sediment age distributions (Figure 10, right side). At the large homogenized increment T_m = 2400 years (Figure 10), the age distribution of the bulk sediment begins to resemble a nonnormal unimodal distribution, but is far from the original component age distributions because considerable blending has occurred.

[31] The age distribution centroids of the falling sediments as well as their relative proportions in Figure 10 were identical to those in calculated from Gaussian decomposition of KC-47 244–245 cm (Figure 10 and Table 3). The widths of the component distributions were chosen on the basis of the assumption that allochthonous organic material (Figure 10, blue and green distributions) is associated with fine particles which have a relatively large lateral component to their settling velocities and are more likely to have been entrained and resettled numerous times. The sharp distribution employed on the youngest sediment component (Figure 10, red distributions) corresponds to a narrower distribution of ages that would best describe a coarse sediment component (such as a foraminiferal test relative to a clay particle) having a similar settling history to organic material which could be considered autochthonous. The model shown Figure 10 does not incorporate differential sedimentation rates, differential bioturbation, nor environmental signals as in the work by *Bard* [2001], but the establishment of first-order effects of bioturbation on different age distributions of sediments within a single historical layer provides a foundation on which to incorporate differential bioturbation approaches with the abundant evidence of differential deposition. With evidence of differentially aged sedimentary components increasing as dating techniques are refined, it is important to provide improved models dealing with signal deconvolution as paleoceanographers and paleoclimatogists aim to compare sedimentary records from different regions during important, dynamic epochs of Earth history.

5. Conclusions

[32] Incremental pyrolysis can be used to improve upon bulk chronology of organic material in sediments that contain components from a spectrum of ages. The geologic implications of this advance are significant in light of our critical assessment of

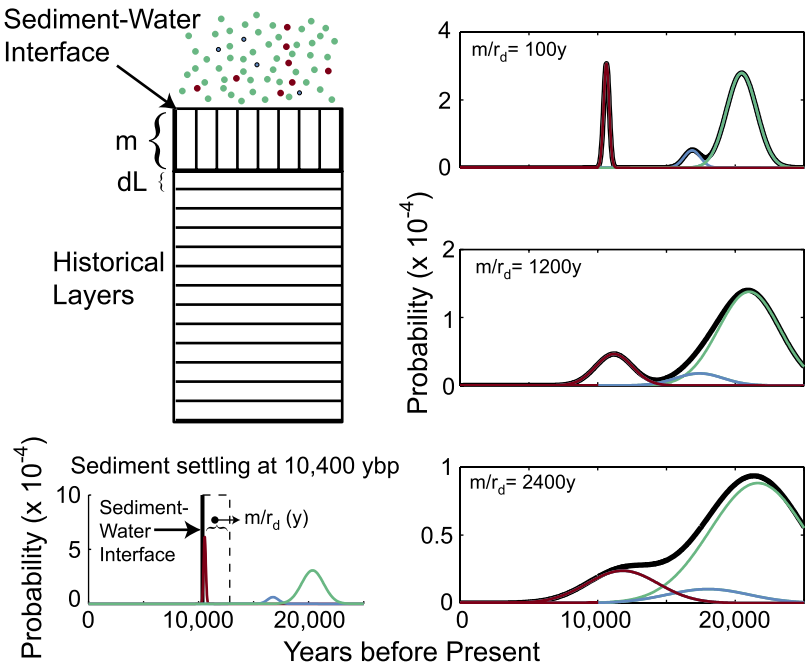

Figure 10. Bioturbation scenarios for coevally deposited sediment components having different age distributions. The left of the figure shows the age distribution of three different particle types (bottom) with notation based on Figure 1 of *Berger and Heath* [1968] (top left). The right of the figure displays the age distribution of sediments taken from this layer after deposition from the homogeneous layer m into the historical layers, assuming constant deposition rate. The three probability density functions on the right (thick black lines represent sum of three components, shown in respective colors) correspond to bulk age distributions of different homogeneous increments as determined by the relation m/r_d (see text).

both the limitations and promise of this method. Analysis of the samples at a higher resolution will likely improve our understanding of the low-temperature ages of the sediments; however, a first-order estimation of the low-temperature cutoff illustrates the difficulties associated with observing a low-temperature age plateau. Recent developments in AMS techniques may enable this approach in a more practical sense [*Roberts et al.*, 2003, 2007]; however, these methods are not currently available. Information about the pyrolysis kinetics of major components in sediment would be beneficial in constructing multicomponent mixing models of the actual ages of the components and re-evaluating our estimate of the low-temperature cutoff. A well-designed test of our reaction kinetics assumption in conjunction with higher-resolution analysis of the low-temperature components would enable further improvement on sediment chronologies using this technique. This work, in light of similar findings from studies of component ages within sediment horizons, suggests a new model for both deposition and bioturbation of marine sediments that will enable deconvolution of complimentary analytical methods carried out on different components in the same sediment core.

Acknowledgments

[33] The authors wish to acknowledge positive reviews from Jeff Pigati and an anonymous reviewer. In addition to the reviewers' suggestions, Laurent Labeyrie played a large role in shaping this article as editor. The authors wish to thank the Sample Preparation Laboratory of NOSAMS at WHOI for their hard work in turning these samples around very quickly. The project was paid for in part by NSF research grants OPP 02-30089 and OPP 03-38142 to Hamilton College (E. Domack) and NSF Cooperative Agreement OCE-0228996 to Woods Hole Oceanographic Institution.

References

Andrews, J. T., E. W. Domack, W. L. Cunningham, A. Leventer, K. J. Licht, A. J. T. Jull, D. J. DeMaster, and A. E. Jennings (1999), Problems and possible solutions concerning radiocarbon dating of surface marine sediments, Ross Sea, Antarctica, *Quat. Res.*, *52*, 206–216.

Backman, E., and E. W. Domack (2003), Depositional architecture and seafloor mapping of the Vega Drift, Erebus and Terror Gulf, Antarctic Peninsula, *Eos Trans. AGU*, *84*(46), Abstract PP31B-0256.

Bard, E. (2001), Paleoceanographic implications of the difference in deep-sea sediment mixing between large and fine particles, *Paleoceanography*, *16*(3), 235–239.

Berger, W. H., and G. R. Heath (1968), Vertical mixing in pelagic sediments, *J. Mar. Res.*, *26*(2), 134–143.

Camerlenghi, A., E. Domack, M. Rebesco, R. Gilbert, S. Ishman, A. Leventer, S. Brachfeld, and A. Drake (2001), Glacial morphology and post-glacial contourites in northern Prince Gustav Channel (NW Weddell Sea, Antarctica), *Mar. Geophys. Res.*, *22*, 417–443.

Cramer, B. (2004), Methane generation from coal during open system pyrolysis investigated by isotope specific, Gaussian distributed reaction kinetics, *Org. Geochem.*, *35*, 379–392.

Darwin, C. (1881), *The Formation of Vegetable Mould Through the Action of Worms With Observation of Their Habits*, 328 pp., John Murray, London.

DeMaster, D. J., O. Ragueneau, and C. A. Nittrouer (1996), Preservation efficiencies and accumulation rates for biogenic silica and organic C, N, and P in high-latitude sediments: The Ross Sea, *J. Geophys. Res.*, *101*(C8), 501–518.

Domack, E. W. (1999), Late Pleistocene-Holocene retreat of the West Antarctic Ice-Sheet system in the Ross Sea: Part 2 — Sedimentologic and stratigraphic signature, *Geol. Soc. Am. Bull.*, *111*(10), 1517–1536.

Domack, E. W., A. Leventer, R. B. Dunbar, F. W. Taylor, S. Brachfeld, C. Sjunneskog, and ODP Leg 178 Science Party (2001), Chronology of the Palmer Deep site, Antarctic Peninsula: A Holocene palaeoenvironmental reference for the circum-Antarctic, *Holocene*, *11*(1), 1–9.

Eglinton, T. I., L. I. Aluwihare, J. E. Bauer, E. R. M. Druffel, and A. P. McNichol (1996), Gas chromatographic isolation of individual compounds from complex matrices for radiocarbon dating, *Anal. Chem.*, *68*, 904–912.

Kellogg, T. B., R. S. Truesdale, and L. E. Osterman (1979), Later Quaternary extent of the West Antarctic ice sheet: New evidence from Ross Sea cores, *Geology*, *7*, 249–253.

Licht, K. J., A. E. Jennings, J. T. Andrews, and K. M. Williams (1996), Chronology of the late Wisconsin ice retreat from the western Ross Sea, Antarctica, *Geology*, *24*, 223–226.

Licht, K. J., W. L. Cunningham, J. T. Andrews, E. W. Domack, and A. E. Jennings (1998), Establishing chronologies from acid-insoluble organic ^{14}C dates on Antarctic (Ross Sea) and Arctic (North Atlantic) marine sediments, *Pol. Res.*, *17*, 203–216.

McGeehin, J., G. S. Burr, A. J. T. Jull, D. Reines, J. Gosse, P. T. Davis, D. Muhs, and J. Southon (2001), Stepped-combustion ^{14}C dating of sediment: A comparison with established techniques, *Radiocarbon*, *43*(2A), 255–261.

McGeehin, J., G. S. Burr, G. Hodgins, S. J. Bennett, J. A. Robbins, N. Morehead, and H. Markewich (2004), Stepped-combustion ^{14}C dating of bomb carbon in lake sediment, *Radiocarbon*, *46*(2), 893–900.

Mollenhauer, G., and T. I. Eglinton (2007), Diagenetic and sedimentological controls on the composition of organic matter preserved in California Borderland Basin sediments, *Limnol. Oceanogr.*, *52*(2), 558–576.

Mollenhauer, G., G. Eglinton, N. Ohkouchi, R. R. Schneider, P. J. Müller, P. M. Grootes, and J. Rullkötter (2003), Asynchronous alkenone and foraminifera records from the Benguela Upwelling System, *Geochim. Cosmochim. Acta*, *67*(12), 2157–2171.

Mollenhauer, G., M. Kienast, F. Lamy, H. Meggers, R. R. Schneider, J. M. Hayes, and T. I. Eglinton (2005), An evaluation of ^{14}C age relationships between co-occurring foraminifera, alkenones, and total organic carbon in continental margin sediments, *Paleoceanography*, *20*, PA1016, doi:10.1029/2004PA001103.

Mollenhauer, G., J. F. McManus, A. Benthien, P. J. Müller, and G. Eglinton (2006), Rapid lateral particle transport in the Argentine Basin: Molecular ^{14}C and $^{230}Th_{xs}$ evidence, *Deep Sea Res., Part I*, *53*, 1224–1243.

Ohkouchi, N. (2003), Radiocarbon dating of individual fatty acids as a tool for refining Antarctic margin sediment chronologies, *Radiocarbon*, *45*(1), 17–23.

Ohkouchi, N., and T. I. Eglinton (2006), Radiocarbon constraint on relict organic carbon contributions to Ross Sea sediments, *Geochem. Geophys. Geosyst.*, *7*, Q04012, doi:10.1029/2005GC001097.

Ohkouchi, N., T. I. Eglinton, S. P. Sylva, C. Thornton, E. Domack, and J. M. Hayes (2000), New approaches to radiocarbon dates in Antarctic coastal sediments, *Eos Trans. AGU*, *81*(48), Fall Meet. Suppl., Abstract U22B-02.

Roberts, M., A. Benthien, R. J. Schneider, K. F. von Reden, and J. M. Hayes (2003), Continuous-flow accelerator Mass Spectrometry, paper presented at 1st International Symposium on Radiation Physics, pp. 7, Int. Radiat. Phys. Soc., Mexico City.

Roberts, M. L., R. J. Schneider, K. F. von Reden, J. S. C. Wills, B. X. Han, J. M. Hayes, B. E. Rosenheim, and W. J. Jenkins (2007), Progress on a gas-accepting ion source for continuous-flow accelerator mass spectrometry, *Nucl. Instrum. Methods Phys. Res., Sect. B*, *259*(1), 83–87.

Roe, K. M., S. Sylva, and E. W. Domack (2006), Particulate carbon distribution and composition beneath ice shelves: Examples from the Larsen system, Antarctica, *Geol. Soc. Am. Abstr. Programs*, *38*, 482.

Villinski, J. C., J. M. Hayes, S. C. Brassell, V. L. Riggert, and R. B. Dunbar (2008), Sedimentary sterols as biogeochemical indicators, *Organic Geochemistry*, in press.